Optimal Charging of Li-Ion Batteries with Coupled Electro-Thermal-Aging Dynamics

H. E. Perez*, *Student Member, IEEE*, X. Hu*, *Member, IEEE*,
S. Dey, *Member, IEEE*, and S. J. Moura, *Member, IEEE*

***Abstract*—Fast and safe charging protocols are crucial for enhancing the practicality of batteries, especially for mobile applications such as smartphones and electric vehicles. This paper proposes an innovative approach to devising optimally health-conscious fast-safe charge protocols. A multi-objective optimal control problem is mathematically formulated via a coupled electro-thermal-aging battery model, where electrical and aging sub-models depend upon the core temperature captured by a two-state thermal sub-model. The Legendre-Gauss-Radau (LGR) pseudo-spectral method with adaptive multi-mesh-interval collocation is employed to solve the resulting highly nonlinear six-state optimal control problem. Charge time and health degradation are therefore optimally traded off, subject to both electrical and thermal constraints. Minimum-time, minimum-aging, and balanced charge scenarios are examined in detail. Sensitivities to the upper voltage bound, ambient temperature, and cooling convection resistance are investigated as well. Experimental results are provided to compare the tradeoffs between a balanced and traditional charge protocol.**

***Index Terms*—Battery Management, Charge Control Optimization, Electric Vehicles, Battery Aging, Experimental Validation.**

I. Introduction

BATTERIES are widely used in mobile handsets, electric vehicles (EVs), and electric grid energy storage. They are an enabling technology for diversifying and securing our future energy supplies. In contrast to simple and rapid refueling of gasoline or diesel, battery recharge requires meticulous control and management, owing to complex electrochemical reactions, immeasurable internal states, and serious safety concerns [1]. Fast charging is a thriving area of research, as it increases the practicality and consumer acceptance of battery-powered devices (e.g., EVs). Nevertheless, it can also impair battery longevity depending on the charging method used, particularly due to heating. It is thus crucial to systematically study the tradeoffs between charging time and health degradation, which is the focus of this paper.

The traditional charging protocol for Li-ion batteries is constant-current/constant-voltage (CCCV) [2]. In the CC stage, the charging current is constant until a pre-specified voltage threshold is reached; in the CV stage the voltage threshold is maintained until the current relaxes below a pre-specified threshold value. This technique is simple and easily implemented. The current rate and voltage threshold are, however, almost universally selected in an ad-hoc manner.

Various methods were proposed to reduce charge times. Examples include multi-stage CC (high CC followed by low CC) plus CV (MCC-CV) [3], fuzzy logic [4], [5], neural networks [6], grey system theory [7], and an ant colony system algorithm [8]. Alternative protocols were reported to prolong the battery lifetime as well, such as MCC-CV (low CC followed by high CC plus CV) [9] and CCCV with negative pulse (CCCV-NP) [10]. These protocols are almost always heuristic. That is, they employ basic knowledge or empirical observations of electrical properties of batteries to devise a charging strategy. Their implementation and performance are subject to cumbersome meta-parameter tuning. Furthermore, there are no mathematical guarantees for fast charge optimality or safe constraint satisfaction.

Recently, some researchers have given first insights into model-based optimal charge control [11]–[16]. A significant challenge for model-based charge control is numerically solving a multi-state nonlinear calculus of variations optimal control problem. These previous studies side-step this difficulty using linear-quadratic formulations [11], state-independent electrical parameters [12], piecewise constant time discretization [13], linear input-output models [14], a one-step model predictive control formulation [15], or a reference governor formulation [16]. To directly face the nonlinear variational calculus problem, orthogonal collocation enabled pseudo-spectral methods were employed in [17] to optimize charging time and efficiency of lithium-ion batteries. However, all of the foregoing studies merely consider the electrical behavior of batteries, without simultaneously accounting for thermal and aging dynamics. Consequently, the optimized protocols may markedly deviate from reality, as batteries invariably work at varying thermal and aging conditions. Moreover, one cannot explore aging minimization and temperature-related safety considerations (e.g., thermal runaway).

This paper pursues a different approach to developing optimally health-conscious fast-safe charging protocols. Mathematically, we formulate a multi-objective optimal control problem via a coupled electro-thermal-aging model. In the full model, a two-state thermal subsystem captures both core and surface temperature dynamics. The core temperature feeds into parameters within the electrical and aging subsystems [18]. Due to the bi-directional coupling between subsystems, the optimization problem is highly nonlinear. Consequently,

 This work was supported in part by the National Science Foundation under Grant No. 1408107.
(*Corresponding authors: H. E. Perez and X. Hu).

H. E. Perez, S. Dey, and S. J. Moura are with the Energy, Controls, and Applications Lab, Department of Civil and Environmental Engineering, University of California, Berkeley, CA 94720, USA (E-mail: {heperez, satadru86, smoura}@berkeley.edu).

X. Hu is with The State Key Laboratory of Mechanical Transmissions, College of Automotive Engineering, Chongqing University, Chongqing 400044, China (E-mail: xiaosonghu@ieee.org).

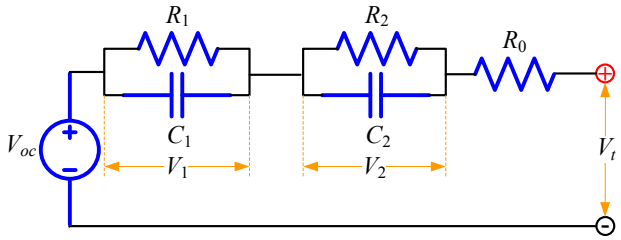

Fig. 1. Schematic of the Electrical Model.

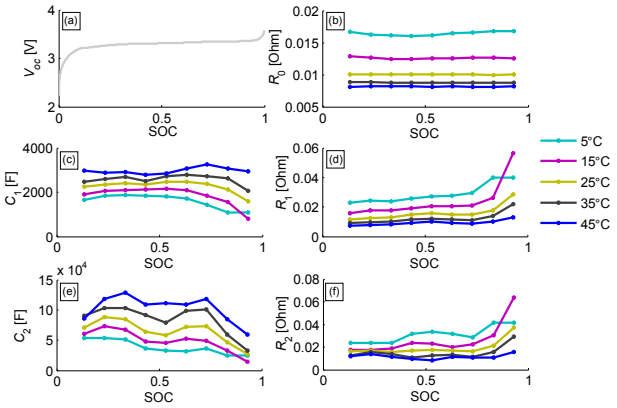

Fig. 2. Electrical Parameters for Charge identified in [18]: (a) V_{oc}, (b) R_0, (c) C_1, (d) R_1, (e) C_2, and (f) R_2.

there are no analytic solutions and numerical solutions have been previously considered intractable. We challenge this entrenched mindset by leveraging the Legendre-Gauss-Radau (LGR) pseudo-spectral method with adaptive multi-mesh-interval collocation. To the best of our knowledge, it is the first multi-objective optimization framework for optimally trading off charging time and battery capacity fade, subject to both electrical and thermal limits. It is also worth highlighting that incorporating a two-state temperature model in lieu of the commonly-used single lumped temperature yields more accurate predictions and safer charging protocols since it is known that the core temperature can be higher than the surface temperature under high current rates (experimentally shown in [18]). Additionally, a two RC pair electrical model is used which provides the right balance between complexity and accuracy (as demonstrated in [18]) required to capture the voltage dynamics under several operating conditions. This article extends our previous work [19] with: (i) an experimental validation of the electro-thermal model dynamics for charging, (ii) analysis of optimal charge protocols using the aging model coupled to the validated electro-thermal model, and (iii) experimental comparison and tradeoff analysis of capacity fade and charging time for a balanced charge and traditional CCCV protocol.

The remainder of this paper is structured as follows. In Section II, the coupled electro-thermal-aging model is described. In Section III, the multi-objective optimal control problem is formulated, and the LGR pseudo-spectral method is briefly introduced. Optimization results are discussed in Section IV, followed by experimental results in Section V. Finally, Section VI summarizes the key findings.

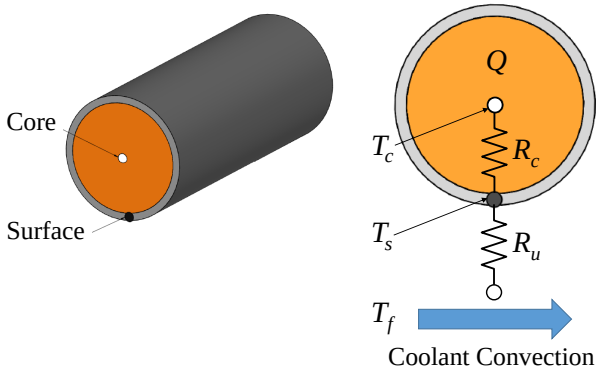

Fig. 3. Schematic of the Thermal Model (adopted from [18]).

II. Coupled Electro-Thermal-Aging Model

In this section, a coupled electro-thermal-aging model is described for cylindrical lithium-iron-phosphate batteries (A123 ANR26650M1). It consists of a second-order equivalent circuit model for emulating voltage behavior, a two-state thermal model for predicting the core and surface temperatures, and a semi-empirical capacity-fade model. The electrical parameters depend upon core temperature, SOC, and current direction. The thermal parameters are constant. The parameters of the aging model depend upon current rate and core temperature. None of the individual subsystem models are new, yet their integration into optimal charging control is novel.

A. Electrical Model

The electrical model in Fig. 1 comprises an open-circuit voltage (OCV, V_{oc}), two resistor-capacitor (RC) pairs (R_1, C_1, R_2, C_2), and an ohmic resistor (R_0). The state-space model is given by:

$$\frac{dSOC}{dt}(t) = \frac{I(t)}{C_{bat}}, \quad (1)$$

$$\frac{dV_1}{dt}(t) = -\frac{V_1(t)}{R_1C_1} + \frac{I(t)}{C_1}, \quad (2)$$

$$\frac{dV_2}{dt}(t) = -\frac{V_2(t)}{R_2C_2} + \frac{I(t)}{C_2}, \quad (3)$$

$$V_t(t) = V_{oc}(SOC) + V_1(t) + V_2(t) + R_0I(t), \quad (4)$$

where C_{bat} is the nominal capacity, $I(t)$ is the current (positive for charge), and $V_t(t)$ denotes the terminal voltage. The three states include SOC and voltages (V_1, V_2) across the two RC pairs. Through proper experimental design, the electrical parameters have been successfully identified in [18], and those for charge are displayed in Fig. 2. We determine V_{oc} using our experimental setup as described in Section V.

B. Thermal Model

The thermal model sketched in Fig. 3 describes the radial heat transfer dynamics of a cylindrical battery by considering core and surface temperatures T_c and T_s as follows:

$$\frac{dT_c(t)}{dt} = \frac{T_s(t) - T_c(t)}{R_cC_c} + \frac{Q(t)}{C_c}, \quad (5)$$

TABLE I
THERMAL PARAMETERS.

$R_c(KW^{-1})$	$R_u(KW^{-1})$	$C_c(JK^{-1})$	$C_s(JK^{-1})$
1.94	3.08	62.7	4.5

TABLE II
PRE-EXPONENTIAL FACTOR AS A FUNCTION OF THE C-RATE.

C-rate c	0.5	2	6	10
M	31630	21681	12934	15512

$$\frac{dT_s(t)}{dt} = \frac{T_f(t) - T_s(t)}{R_u C_s} - \frac{T_s(t) - T_c(t)}{R_c C_s}, \quad (6)$$

where $Q(t) = |I(V_{oc} - V_t)|$ is heat generation including joule heating and energy dissipated by electrode over-potentials. The heat conduction resistance, convection resistance, core heat capacity, and surface heat capacity are represented by R_c, R_u, C_c, and C_s, respectively. The two states are the core T_c and surface T_s temperatures. As treated in [18], we herein assume that the coolant flow rate is constant, and the ambient temperature T_f is nearly constant. The thermal parameters have been calibrated in previous work and are summarized in Table I [18]. We determine R_u using our experimental setup as described in Section V.

We remark that the electro-thermal model has been validated over a broad range of loading conditions covering a maximum current rate up to 22C. More details are furnished in [18] regarding the model topology, parameterization, experimental design for identification, and validations. We validate the effectiveness of the electro-thermal model for a charging case in Section V.

C. Aging Model

We adopt an aging model from [20] that is based upon a matrix of cycling tests. This matrix spans different C-rates[1] (C/2 to 10C), temperatures (-30°C to +60°C), and depths-of-discharge (10% to 90%) for lithium iron phosphate cells (A123 ANR26650M1). The experimental data demonstrates that capacity fade depends strongly on C-rate and temperature in these cells, whereas the sensitivity to depth-of-discharge (DOD) is negligible. However, the DOD effect can be captured by the processed ampere-hour (Ah) throughput as described in Section 3.1 of [20]. A correlation between the capacity loss and the discharged Ah throughput (which also captures the effects of C-rate and temperature) has been calibrated by the following semi-empirical model:

$$\Delta Q_b = M(c) \exp\left(\frac{-E_a(c)}{RT_c}\right) A(c)^z, \quad (7)$$

where ΔQ_b is the percentage of capacity loss in [%], c is the C-rate, and $M(c)$ is the pre-exponential factor as a function of the C-rate, as shown in Table II (from Table 3 of [20]). Symbol R is the ideal gas constant and A is the discharged Ah throughput depending on C-rate. The activation energy E_a in $[Jmol^{-1}]$ and the power-law factor z are given by

$$E_a(c) = 31700 - 370.3c, \qquad z = 0.55. \quad (8)$$

[1]C-rate is a normalized measure of electric current, defined as the ratio of current $I(t)$ in Amperes, to a cell's nominal capacity C_{bat} in Ampere-hours.

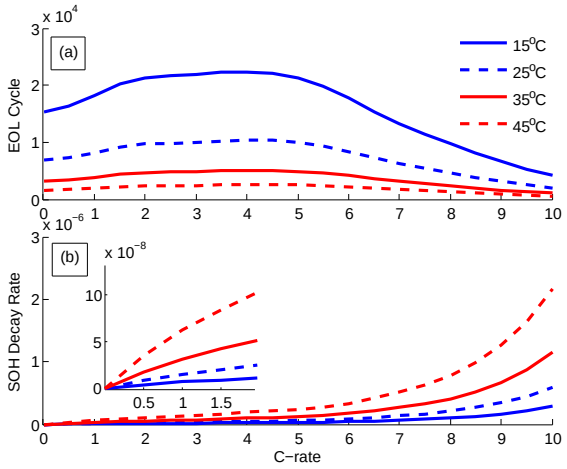

Fig. 4. Battery SOH Model: (a) EOL Cycle $N(c, T_c)$ from Eq. 10, and (b) SOH Decay Rate from Eq. 12 as Functions of C-rate.

A capacity loss of 20% ($\Delta Q_b = 20\%$) is often indicative of the end-of-life (EOL) for an automotive battery, and the corresponding total discharged Ah throughput A_{tol} and number of cycles until EOL, N are algebraically calculated from (7) as

$$A_{tol}(c, T_c) = \left[\frac{20}{M(c)\exp\left(\frac{-E_a(c)}{RT_c}\right)}\right]^{\frac{1}{z}}, \quad (9)$$

$$N(c, T_c) = \frac{3600 A_{tol}(c, T_c)}{C_{bat}}, \quad (10)$$

where each cycle corresponds to $2C_{bat}$ charge throughput. Note that A_{tol} is the discharged Ah throughput used by the aging model in [20], and thus the total throughput should be $2A_{tol}$ including both charged and discharged Ah. Based on (9) and (10), the battery State-of-Health (SOH) can be defined below:

$$SOH(t) = SOH(t_0) - \frac{\int_{t_0}^{t} |I(\tau)| d\tau}{2N(c, T_c) C_{bat}}, \quad (11)$$

where t_0 denotes the initial time. Consequently, $SOH = 1$ corresponds to a fresh battery and $SOH = 0$ corresponds to 20% capacity loss. The time derivative of (11) yields the battery aging model

$$\frac{dSOH}{dt}(t) = -\frac{|I(t)|}{2N(c, T_c) C_{bat}}. \quad (12)$$

The EOL cycle and SOH decay rate, as a function of the C-rate and core temperature, are visualized in Fig. 4. As the C-rate or core temperature increases, the SOH decay rate increases. It is worth pointing out that more EOL cycles can be sustained by the battery at medium C-rates (2-5C) than at low C-rates, as the

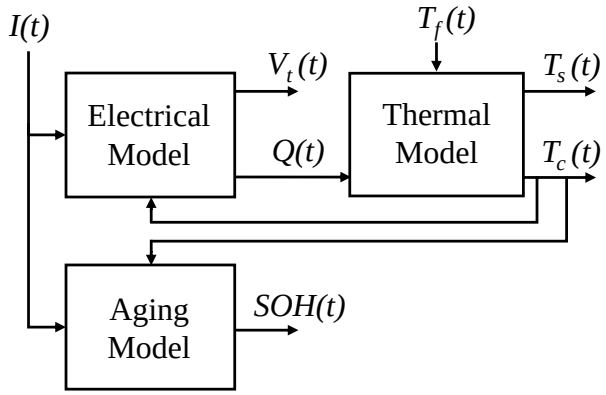

Fig. 5. Electro-Thermal-Aging Model Coupling.

aging model includes calendar-life effects as well (one cycle at a very low C-rate has a dramatically increased duration). The effects of calendar life are embedded into the aging model in the Ah throughput calculation which is directly proportional to time according to [20]. Note that this model considers aging during periods of applied current, and the results should be understood as such. The aging model validated in [20] has been similarly applied to health-conscious component sizing and energy management in hybrid electric vehicles [21].

D. Full Model

Combining the above three sub-models produces the coupled electro-thermal-aging model (block diagram in Fig. 5) used for the subsequent charging protocol optimization. The model dynamics are summarized in (13)-(18), with output equation (4).

$$\frac{dSOC}{dt}(t) = \frac{I(t)}{C_{bat}}, \tag{13}$$

$$\frac{dV_1}{dt}(t) = -\frac{V_1(t)}{R_1C_1} + \frac{I(t)}{C_1}, \tag{14}$$

$$\frac{dV_2}{dt}(t) = -\frac{V_2(t)}{R_2C_2} + \frac{I(t)}{C_2}, \tag{15}$$

$$\frac{dT_c}{dt}(t) = \frac{T_s(t)-T_c(t)}{R_cC_c} + \frac{I(t)(V_1(t)+V_2(t)+R_0I(t))}{C_c}, \tag{16}$$

$$\frac{dT_s}{dt}(t) = \frac{T_f(t)-T_s(t)}{R_uC_s} - \frac{T_s(t)-T_c(t)}{R_cC_s}, \tag{17}$$

$$\frac{dSOH}{dt}(t) = -\frac{|I(t)|}{2N(c,T_c)C_{bat}}. \tag{18}$$

III. Formulation of Optimal Charge Control

The objective function J combines charge time with capacity loss (i.e. SOH decay) as follows:

$$\min_{I(t),x(t),t_f} \quad J = \beta\cdot\frac{t_f-t_0}{t_{\max}-t_0} + (1-\beta)\cdot(SOH(t_0)-SOH(t_f)), \tag{19}$$

where t_f is the final time of charge and $0 \le \beta \le 1$ weights the relative importance between the two objectives. The optimization variables are the input current $I(t)$, state variables $x(t) = [SOC(t), V_1(t), V_2(t), T_c(t), T_s(t), SOH(t)]^T$, and final time t_f. The constraints include the model dynamics (13)-(18) and the electrical, thermal, health, and time limits below:

$$SOC_{\min} \le SOC \le SOC_{\max}, \qquad I_{\min} \le I \le I_{\max}, \tag{20}$$

$$SOC(t_0) = SOC_0, \qquad V_{t,\min} \le V_t \le V_{t,\max}, \tag{21}$$

$$SOC(t_f) = SOC_f, \qquad T_{c,\min} \le T_c \le T_{c,\max}, \tag{22}$$

$$SOH_{\min} \le SOH \le SOH_{\max}, \qquad SOH(t_0) = SOH_0, \tag{23}$$

$$T_c(t_0) = T_{c,0}, T_s(t_0) = T_{s,0}, \qquad t_0 \le t \le t_{\max}. \tag{24}$$

Since the optimal control problem has six states and is highly nonlinear, it is difficult to use conventional optimization techniques, e.g., dynamic programming, Pontryagin's minimum principle, and indirect methods, due to intractable computational burden or complexity. Instead, we pursue pseudo-spectral methods to transcribe this infinite-dimensional optimal control problem into a finite-dimensional optimization problem with algebraic constraints at the discretized nodes. Then, the optimization variables at such nodes are solved by existing nonlinear programming (NLP) solvers, like SNOPT or IPOPT [22]. Note that convexity is not guaranteed, and therefore these solvers yield locally optimal solutions.

Pseudo-spectral methods are an effective tool for complex nonlinear optimal control problems and have been extensively applied to real-world optimization problems in engineering. Examples include aerospace and autonomous flight systems [23], road vehicle systems [24], energy storage [17], etc. There are a myriad of approaches for discretizing integral and differential equations, leading to a spectrum of pseudo-spectral variants. In this study, we use the Legendre-Gauss-Radau (LGR) pseudo-spectral method with adaptive multi-mesh-interval collocation, featured by the general purpose optimal control software (GPOPS-II) [22]. This software incorporates an orthogonal collocation method to generate the LGR points. Rather than a traditional fixed global mesh, an adaptive mesh refinement algorithm is employed to iteratively adjust the number of mesh intervals, the width of each interval, and the polynomial degree (the number of LGR points). More theoretical and algorithmic properties of this method and GPOPS-II are elaborated in [25], [26] and in the Appendix of [19].

IV. Optimization Results and Discussion

This section presents optimization results for three illustrative charge paradigms: minimum-time charge, minimum-aging charge, and balanced charge. These results are presented under the assumption of no modeling, measurement, or control uncertainty. Furthermore, the aging results represent the effects of applying the resulting charge protocols during their respective charge durations. The physical bounds in (20)-(24) and ambient temperature T_f are specified as follows:

$$SOC_{\min} = SOC_0 = 0.25, \quad SOC_{\max} = SOC_f = 0.75, \tag{25}$$

$$I_{\min} = 0A = 0C, \qquad I_{\max} = 46A = 20C, \tag{26}$$

$$V_{t,\min} = 2V, \qquad V_{t,\max} = 3.6V, \tag{27}$$

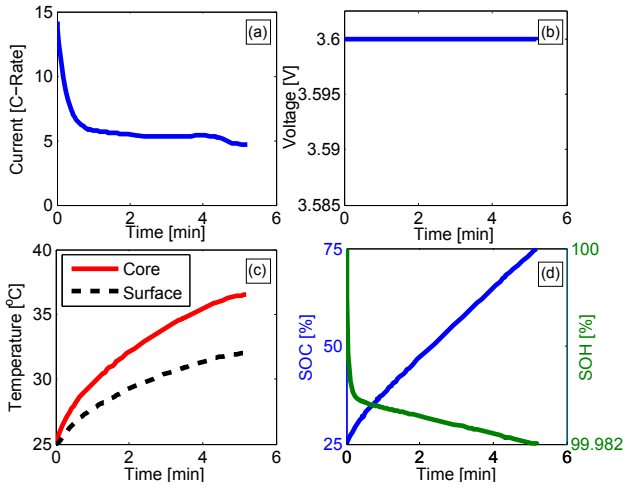

Fig. 6. Optimization Result for the Minimum-Time Charge: (a) C-rate, (b) Terminal Voltage, (c) Core and Surface Temperatures, and (d) SOC/SOH.

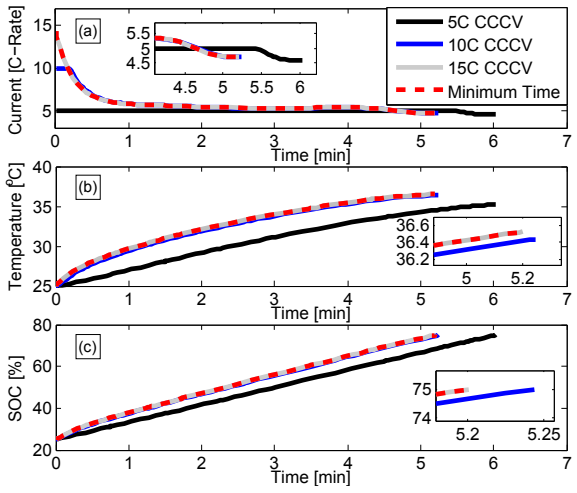

Fig. 7. Comparison with CCCV Charge: (a) C-rate, (b) Core Temperature, and (c) SOC.

$$T_{c,\min} = 5^\circ C, \qquad T_{c,\max} = 45^\circ C, \tag{28}$$

$$T_{c,0} = T_{f,0} = 25^\circ C, \qquad T_f(t) = 25^\circ C, \forall t \geq t_0, \tag{29}$$

$$SOH_{\min} = 0, \qquad SOH_{\max} = SOH_0 = 1, \tag{30}$$

$$t_0 = 0sec, \qquad t_{\max} = 36000sec. \tag{31}$$

Here, the voltage limits are selected according to the manufacturer's specification sheet, and the temperature and current limits are chosen based on the validated range in [18]. The initial condition is chosen slightly above 20% SOC since this is where most consumer electronics begin to indicate to the user that the battery is low, and the final condition of 75% SOC is chosen to represent where the battery would have enough charge to complete desired tasks before the next charge with a minimum time charge time close to 5 minutes (e.g. time it takes to get a cup of coffee while phone is charging or time it takes to refuel a gasoline powered vehicle).

A. Minimum-Time Charge

By setting $\beta = 1$, the optimization produces a minimum-time charge protocol. The optimal trajectories are shown in Fig. 6.

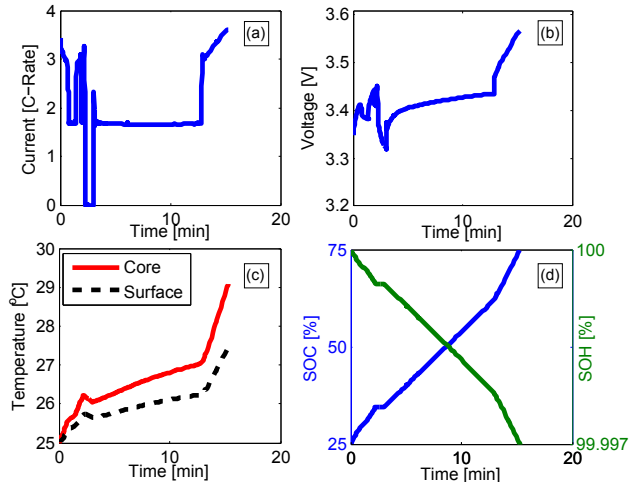

Fig. 8. Optimization Result for the Minimum-Aging Charge: (a) C-rate, (b) Terminal Voltage, (c) Core and Surface Temperatures, and (d) SOC/SOH.

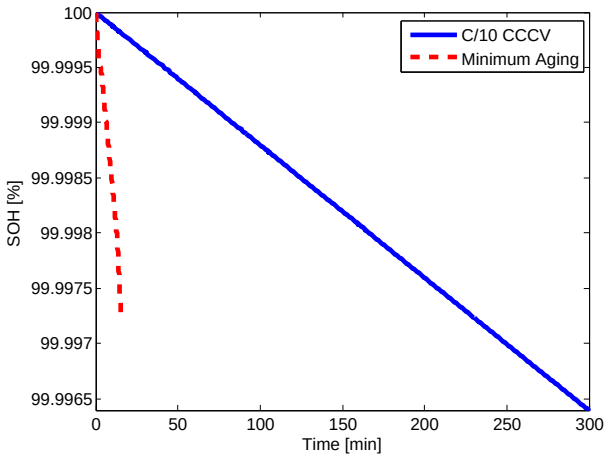

Fig. 9. SOH Trajectories of the Minimum-Aging Charge and C/10 CCCV Charge.

It takes 5.20 minutes to achieve the target SOC. Heuristically, the charge process follows a constant-voltage (CV) protocol. To minimize charging time, the maximum C-rate is applied initially, causing the maximum voltage constraint to become active instantaneously. The core temperature increases but does not reach its maximum value.

A comparison is made with CCCV charges with varying C-rates (see Fig. 7). It is clear that 5C and 10C CCCV are sub-optimal with respect to minimum time charging. The 5C CCCV case yields a 6.04 minute charge time, while the 10C CCCV case yields a 5.24 minute charge time. We note that the 15C CCCV case is exactly the optimal solution. In other words, this analysis yields the insight that CCCV with 15C is optimal in the sense of minimizing charge time. While the constant current rate of this protocol may seem very high, the resulting average C rate is 5.77C which is not far from the recommended CCCV fast charge constant current rate of 10A (4.35C) given by the manufacturer specification sheet of this cell.

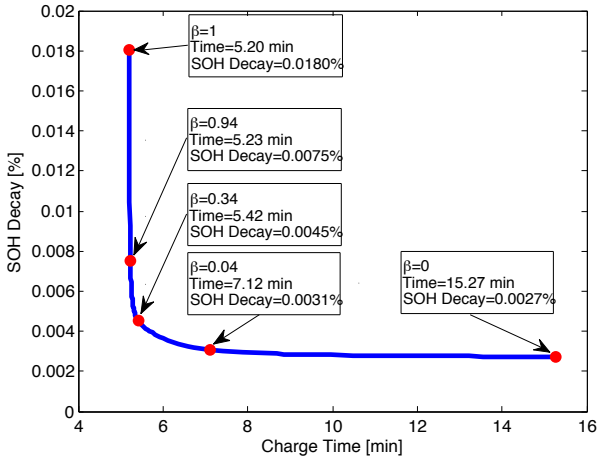

Fig. 10. Pareto Frontier, Charge Time Versus SOH Decay.

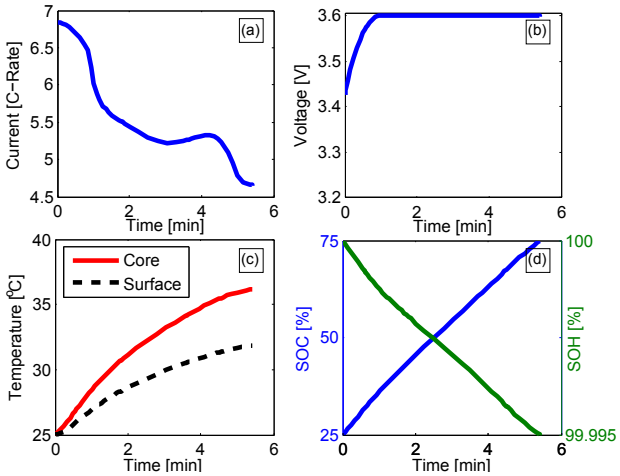

Fig. 11. Optimization Result for the Balanced Charge ($\beta = 0.34$): (a) C-rate, (b) Terminal Voltage, (c) Core and Surface Temperatures, and (d) SOC/SOH.

B. Minimum-Aging Charge

By setting $\beta = 0$, we can investigate the other extreme – a minimum aging charge protocol. The optimization result is illustrated in Fig. 8. Interestingly, the protocol is pulse-like, while maintaining relatively low core temperature. The resulting SOH decay is approximately 0.0027%, one order of magnitude less than the SOH decay from minimum-time charging (SOH decay of approximately 0.0180%). As shown in Fig. 9, a comparison is performed with a C/10 CCCV charge that is widely perceived as a minimum-aging choice. Under the models considered here, the relatively slow C/10 CCCV charge is in fact non-optimal, since the long charge duration significantly contributes to calendar-life decay.

C. Balanced Charge

By sweeping β values between 0 and 1, we compute a Pareto Frontier of balanced charge protocols, i.e., the optimal tradeoffs between fast charge time and SOH decay displayed in Fig. 10. Not surprisingly, the two objectives conflict. Consider the region between the left two data labels in Fig. 10. Battery SOH decay can be substantially mitigated with a negligible

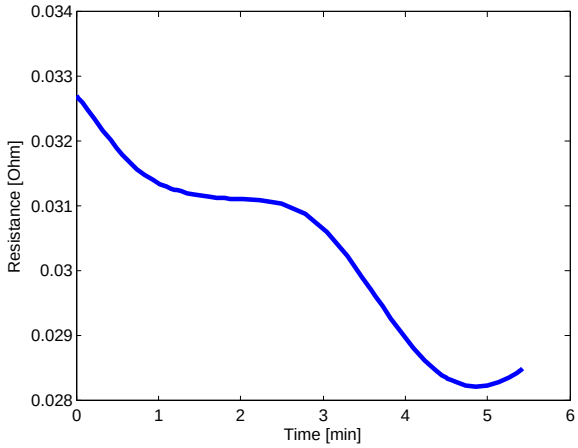

Fig. 12. Trajectory of the Total Equivalent Resistance ($R_0 + R_1 + R_2$) for Balanced Charge ($\beta = 0.34$).

increase in charge time. Therefore, one may sacrifice a trivial amount of fast charge time to circumvent rapid SOH decay.

A "balanced" protocol ($\beta = 0.34$) is exemplified in Fig. 11, which can be interpreted as the smallest-aging solution in the case of 5.42-minute charge duration. Note the highly non-intuitive nature of this charging protocol. The current is carefully regulated to limit the increase of core temperature (a dominant accelerating factor of capacity fade). That is, the current reduces in the first minute to slow down the temperature rise until the voltage constraint becomes active. Next the current decreases at a lower rate since the resistance has decreased (see Fig. 12), and then increases as the resistance continues to decrease in the vicinity of the smallest resistance (due to the increase in temperature). Ultimately the current reduces with the growing resistance towards the higher SOC region. The optimal solution exploits nonlinear model dependencies between resistance and SOC to improve charge time and SOH decay.

D. Sensitivity of Pareto Frontier

Next we examine solution sensitivity to perturbations in the constraint parameters to demonstrate the effects on charge time and aging from a coupled electro-thermal-aging model based perspective. These results are presented to help quantify these effects via the Pareto Frontier plots.

1) Upper Voltage Bound $V_{t,\max}$: The impact of the upper voltage bound $V_{t,\max}$ on the Pareto Frontier is shown in Fig. 13 (Top). As $V_{t,\max}$ decreases, the Pareto Frontier moves to the upper-right and shrinks, resulting in reduced control flexibility. Diminishing $V_{t,\max}$ is therefore unfavorable to the control objective of charge time reduction. For example, compared to $V_{t,\max} = 3.6V$, the minimum charge time increases to 5.87 minutes (12.73% increase) and 6.69 minutes (28.55% increase) in the cases of $V_{t,\max} = 3.575V$ and $V_{t,\max} = 3.55V$, respectively. Not surprisingly, decreasing $V_{t,\max}$ does lead to reduced aging.

2) Ambient Temperature T_f: The impact of the ambient temperature T_f is shown in Fig. 13 (Middle). At low ambient temperature ($T_f = 15°C$), the battery SOH decays slower,

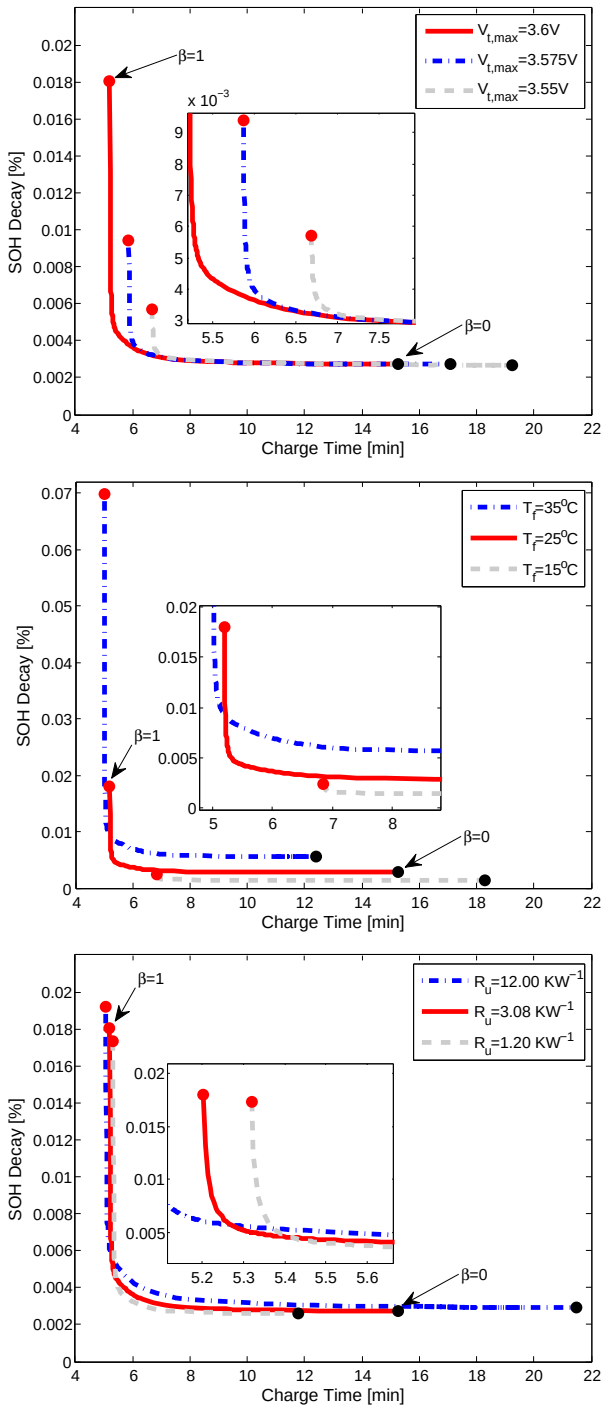

Fig. 13. Top: Influence of $V_{t,\max}$ on Pareto Frontier. Middle: Influence of T_f on Pareto Frontier. Bottom: Influence of R_u on Pareto Frontier.

whereas the minimum charge time increases due to greater internal resistance. That is, the maximum voltage is reached sooner, because of higher ohmic overpotential. At high ambient temperature ($T_f = 35°C$), the battery SOH decays faster, and the minimum charge time decreases because the resistance is decreased due to the higher temperature which allows for higher currents to be applied, compared to the ambient temperature. To summarize, higher ambient temperature favors charging time but also accelerates aging.

3) Cooling Convection Resistance R_u: The impact of cooling convection resistance R_u is shown in Fig. 13 (Bottom). Given a relatively large R_u (representing natural convection), the battery SOH decays faster, and the minimum charge time decreases due to decreased resistance at higher temperature, thus allowing for higher currents. In the case of $R_u = 1.20KW^{-1}$(forced convection), the battery SOH decay is alleviated, but the minimum charge time increases because internal resistance increases as the core temperature decreases, compared to the case of $R_u = 3.08KW^{-1}$. Therefore, we find that increasing the cooling convection resistance decelerates aging yet increases charge time. These sensitivity analyses demonstrate that optimal charging protocols critically depend on the coupled temperature-aging dynamics.

E. Further Discussion

The influence of battery aging on the electrical parameters is not addressed in this work, as it has a substantially longer time scale than the SOC and thermal dynamics. While a fresh battery ($SOH_0 = 1$) is herein considered before charge, the proposed optimization framework applies to different aging levels, provided that the associated SOH_0 and electrical parameters (e.g. internal resistance) are available via recalibration or adaptive estimation [27], [28]. These parameters can be updated to obtain new charge protocols as the battery ages. It is also important to note that the resulting charge protocols can change if different operating constraints for the cell are required. Additionally, the cell and respective models in this study are chosen to illustrate the potential of the multi-objective optimal control framework for obtaining model-based fast-safe battery charge protocols. Moreover, this framework can be used for any type of cell given the proper models that capture the important dynamics (e.g. electrical, thermal, and aging) for multi-objective battery charging.

V. Experimental Results and Discussion

Various experiments were conducted to validate the electro-thermal model from [18] for a 2.3Ah A123 26650 LiFePO4 battery in our test facility. The cell was placed on an Arbin High Current Cylindrical Cell Holder inside of an ESPEC BTL-433 environmental chamber to regulate the ambient temperature at 25°C. A K-type thermocouple was placed on the surface of the battery to measure T_s. First, the cell was cycled using a $C/20$ CCCV test to identify V_{oc} using a PEC SBT2050 cycler that controls the input current to the battery. Then a scaled US06 charge depleting (CD) drive cycle test was performed to identify the convection resistance R_u for our experimental setup. The resulting balanced charge protocol from the optimization results (using the newly determined V_{oc} and R_u) is then applied to the battery for validation of the electro-thermal model. We experimentally compare the model-based balanced charge protocol and a 5C CCCV charge protocol (C-rate chosen based on higher charge time and lower SOH decay than the balanced charge protocol) on two cells based on the insight obtained in the optimization results. The two cells undergo several hundred charge/discharge cycles to determine the changes in capacity fade and charge time.

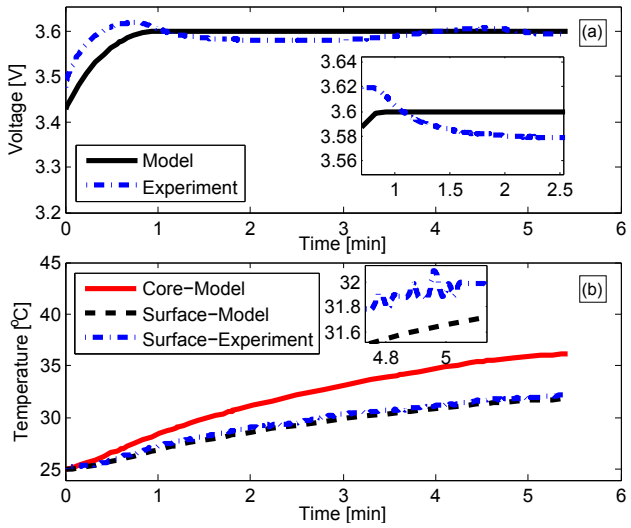

Fig. 14. Experimental Validation of Electro-Thermal Model via Balanced Charge Protocol: (a) Terminal Voltage, and (b) Temperature.

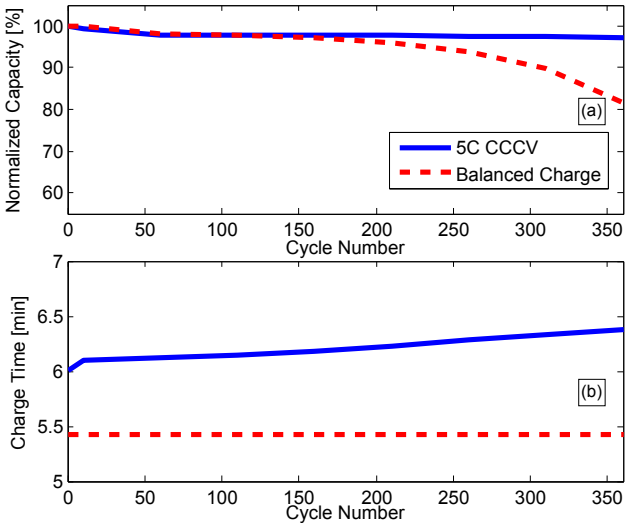

Fig. 15. Balanced and 5C CCCV Charge Protocol Aging: (a) Capacity Fade, and (b) Charge Time.

A. *Electro-Thermal Model Validation*

The open circuit voltage V_{oc} is determined from a C/20 CCCV cycling test (with voltage limits of 3.6V and 2.0V) by taking the average of the charge and discharge voltage curves. The convection resistance R_u is determined from a scaled US06 CD drive cycle applied to a battery at 90% SOC and $25°$C. The final conditions of the drive cycle test are 25% SOC and $32.6°$C with a maximum C-rate of 13.61C. The current for the balanced charge optimization result is then applied (open loop) to validate the electro-thermal model, as shown in Fig. 14 which achieves a Voltage RMSE of 23.6mV and a Surface Temperature RMSE of $0.32°$C.

B. *Charge Protocol Aging*

Two cells were used to determine the tradeoffs between capacity fade and charge time for a fixed 1.15Ah charge throughput using the model-based Balanced charge protocol (from Section IV-C) and the 5C CCCV charge protocol. Both cells are discharged with a 1C CCCV protocol (closed loop) to the open circuit voltage V_{oc} corresponding to 25% SOC until a $C/50$ cutoff current is reached. The charge and discharge protocol of each cell is then repeated for hundreds of cycles. The current from the balanced charge protocol is applied to the first battery cell (open loop). The 5C CCCV charge protocol is applied to the second battery cell (closed loop), using the built-in controller of the battery cycler to maintain the 3.6V limit under the 5C CCCV charge operation. That is, the same current is applied each time for the balanced charge protocol (regardless of what voltage is measured) while the current for the CCCV charge protocol is adjusted in real-time once the voltage constraint becomes active. Therefore, only the 5C CCCV charge protocol will provide compensation as the cell ages.

The discharge capacity is determined using a 1C CCCV cycling test at cycles $\{0, 10, 60, 110, 160, 210, 260, 310, 360\}$ and is shown (normalized against initial capacity) in the first subplot of Fig. 15. The normalized capacity of the balanced charge protocol is 81.64% while that of the 5C CCCV charge protocol is 97.1% at cycle 360. The higher capacity fade experienced by the balanced charge protocol over the full 360 cycles is expected since it is applied in a pure open loop fashion (which does not compensate for the cell going beyond its upper voltage limit as it is cycled) and because it has a faster charge time (which results in more aging per the insight gained in our optimization results). The charge time of the balanced charge protocol stays the same each time while that of the 5C CCCV protocol increases (due to the closed loop compensation which prevents the cell from going beyond its upper voltage limit as it is cycled) as shown in the bottom subplot of Fig. 15. The charge time of the balanced charge protocol is 5.42 minutes while that of the 5C CCCV charge protocol is initially 6.01 minutes. The charge time of the 5C CCCV charge protocol increases to 6.38 minutes at cycle 360. There is a clear tradeoff between degradation and charge time for the applied balanced (open loop) and 5C CCCV (closed loop) charge protocols cycled over time. However, it is important to note that the balanced charge protocol provides a comparable capacity fade to that of the 5C CCCV protocol while maintaining a faster charge time up to cycle 110. These results provide motivation and justification for adaptive optimal charge control to alleviate aging and maintain the desired performance objective over time. Such controller would close the loop and continuously estimate the parameters that age with time to yield accurate model estimates for obtaining new charge protocols as the cell is cycled using the multi-objective optimal control framework presented in this paper.

VI. Conclusions

A multi-objective optimal control framework has been developed to explore model-based fast-safe charging protocols. In this framework, a coupled electro-thermal-aging model is incorporated to account for thermal constraints and aging effects. The Legendre-Gauss-Radau (LGR) pseudo-spectral method with adaptive multi-mesh-interval collocation is lever-

aged to solve the infinite dimensional nonlinear optimal control problem. Charge time and battery capacity fade is traded off, subject to both electrical and thermal constraints, a first to the authors' knowledge. Three charging regimes are analyzed in detail, with the following key findings: (i) Minimum-time charge: the protocol is exactly 15C constant-current/constant-voltage (CCCV), requiring 5.20 minutes to replenish the SOC from 25% to 75%. (ii) Minimum-aging charge: the protocol is pulse-like rather than a slow constant current charge such as C/10 CCCV. The associated SOH decay is 0.0027%, one order of magnitude smaller than that in the minimum-time case. (iii) Balanced charge: the Pareto Frontier demonstrates that a fundamental tradeoff exists between charge time and SOH decay. A slight (even negligible) time increase, relative to the minimum-time case, can significantly alleviate SOH decay. We examine solution sensitivity to variations in several constraint parameters, including maximum voltage, ambient temperature, and cooling convection resistance. This analysis exposes the importance of considering both temperature and aging dynamics for optimal charging. Finally, experimental results of the balanced charge protocol (open loop) versus a 5C CCCV charge protocol (closed loop) are presented with respect to capacity fade and charge time. Future work will close the loop on the optimal charge protocols by combining the coupled electro-thermal-aging model with an adaptive estimator which updates model parameters that change with aging for implementation in real time at our battery in the loop test facility.

REFERENCES

[1] M. Yilmaz and P. Krein, "Review of battery charger topologies, charging power levels, and infrastructure for plug-in electric and hybrid vehicles," *IEEE Trans. on Power Electronics*, vol. 28, no. 5, pp. 2151–2169, May 2013.

[2] S. Zhang, K. Xu, and T. Jow, "Study of the charging process of a licoo2-based li-ion battery," *Journal of Power Sources*, vol. 160, no. 2, pp. 1349 – 1354, 2006, special issue including selected papers presented at the International Workshop on Molten Carbonate Fuel Cells and Related Science and Technology 2005 together with regular papers. [Online]. Available: http://www.sciencedirect.com/science/article/pii/S0378775306004162

[3] D. Ansean, M. Gonzalez, J. Viera, V. Garcia, C. Blanco, and M. Valledor, "Fast charging technique for high power lithium iron phosphate batteries: A cycle life analysis," *Journal of Power Sources*, vol. 239, no. 0, pp. 9 – 15, 2013. [Online]. Available: http://www.sciencedirect.com/science/article/pii/S0378775313004357

[4] H. Surmann, "Genetic optimization of a fuzzy system for charging batteries," *IEEE Trans. on Industrial Electronics*, vol. 43, no. 5, pp. 541–548, Oct 1996.

[5] Y.-H. Liu and Y.-F. Luo, "Search for an optimal rapid-charging pattern for li-ion batteries using the taguchi approach," *IEEE Trans. on Industrial Electronics*, vol. 57, no. 12, pp. 3963–3971, Dec 2010.

[6] Z. Ullah, B. Burford, and S. Dillip, "Fast intelligent battery charging: neural-fuzzy approach," *IEEE Aerospace and Electronic Systems Magazine*, vol. 11, no. 6, pp. 26–34, Jun 1996.

[7] L.-R. Chen, R. Hsu, and C.-S. Liu, "A design of a grey-predicted li-ion battery charge system," *IEEE Trans. on Industrial Electronics*, vol. 55, no. 10, pp. 3692–3701, Oct 2008.

[8] Y.-H. Liu, J.-H. Teng, and Y.-C. Lin, "Search for an optimal rapid charging pattern for lithium-ion batteries using ant colony system algorithm," *IEEE Trans. on Industrial Electronics*, vol. 52, no. 5, pp. 1328–1336, Oct 2005.

[9] S. S. Zhang, "The effect of the charging protocol on the cycle life of a li-ion battery," *Journal of Power Sources*, vol. 161, no. 2, pp. 1385 – 1391, 2006. [Online]. Available: http://www.sciencedirect.com/science/article/pii/S0378775306011839

[10] M. A. Monem, K. Trad, N. Omar, O. Hegazy, B. Mantels, G. Mulder, P. V. den Bossche, and J. V. Mierlo, "Lithium-ion batteries: Evaluation study of different charging methodologies based on aging process," *Applied Energy*, vol. 152, no. 0, pp. 143 – 155, 2015. [Online]. Available: http://www.sciencedirect.com/science/article/pii/S0306261915002494

[11] Y. Parvini and A. Vahidi, "Maximizing Charging Efficiency of Lithium-Ion and Lead-Acid Batteries Using Optimal Control Theory," in *2015 American Control Conference*, Chicago, IL USA, July 1-3 2015.

[12] A. Abdollahi, N. Raghunathan, X. Han, G. V. Avvari, B. Balasingam, K. R. Pattipati, and Y. Bar-Shalom, "Battery Charging Optimization for OCV-Resistance Equivalent Circuit Model," in *2015 American Control Conference*, Chicago, IL USA, 2015.

[13] R. D. B. Ravi Methekar, Venkatasailanathan Ramadesigan and V. R. Subramanian, "Optimum charging profile for lithium-ion batteries to maximize energy storage and utilization," *ECS Trans.*, vol. 25, no. 35, pp. 139–146, 2010.

[14] M. Torchio, N. A. Wolff, D. M. Raimondo, L. Magni, U. Krewer, R. B. Gopaluni, J. A. Paulson, and R. D. Braatz, "Real-time Model Predictive Control for the Optimal Charging of a Lithium-ion Battery," in *2015 American Control Conference*, Chicago, IL USA, 2015.

[15] R. Klein, N. Chaturvedi, J. Christensen, J. Ahmed, R. Findeisen, and A. Kojic, "Optimal charging strategies in lithium-ion battery," in *American Control Conference (ACC), 2011*, June 2011, pp. 382–387.

[16] H. Perez, N. Shahmohammadhamedani, and S. Moura, "Enhanced performance of li-ion batteries via modified reference governors and electrochemical models," *IEEE/ASME Trans. on Mechatronics*, vol. PP, no. 99, pp. 1–10, 2015.

[17] X. Hu, S. Li, H. Peng, and F. Sun, "Charging time and loss optimization for linmc and lifepo4 batteries based on equivalent circuit models," *Journal of Power Sources*, vol. 239, no. 0, pp. 449 – 457, 2013. [Online]. Available: http://www.sciencedirect.com/science/article/pii/S037877531300551X

[18] X. Lin, H. E. Perez, S. Mohan, J. B. Siegel, A. G. Stefanopoulou, Y. Ding, and M. P. Castanier, "A lumped-parameter electro-thermal model for cylindrical batteries," *Journal of Power Sources*, vol. 257, no. 0, pp. 1 – 11, 2014. [Online]. Available: http://www.sciencedirect.com/science/article/pii/S0378775314001244

[19] X. Hu, H. E. Perez, and S. J. Moura, "Battery charge control with an electro-thermal-aging coupling," in *ASME 2015 Dynamic Systems and Control Conference*, Dynamic Systems and Control Division. Columbus, Ohio, USA: ASME, October 2015.

[20] J. Wang, P. Liu, J. Hicks-Garner, E. Sherman, S. Soukiazian, M. Verbrugge, H. Tataria, J. Musser, and P. Finamore, "Cycle-life model for graphite-lifepo4 cells," *Journal of Power Sources*, vol. 196, no. 8, pp. 3942 – 3948, 2011. [Online]. Available: http://www.sciencedirect.com/science/article/pii/S0378775310021269

[21] S. Ebbesen, P. Elbert, and L. Guzzella, "Battery state-of-health perceptive energy management for hybrid electric vehicles," *IEEE Trans. on Vehicular Technology*, vol. 61, no. 7, pp. 2893–2900, Sept 2012.

[22] M. A. Patterson and A. V. Rao, "Gpops-ii: A matlab software for solving multiple-phase optimal control problems using hp-adaptive gaussian quadrature collocation methods and sparse nonlinear programming," *ACM Trans. on Mathematical Software (TOMS)*, vol. 41, no. 1, 2014.

[23] I. M. Ross and M. Karpenko, "A review of pseudospectral optimal control: From theory to flight," *Annual Reviews in Control*, vol. 36, no. 2, pp. 182 – 197, 2012. [Online]. Available: http://www.sciencedirect.com/science/article/pii/S1367578812000375

[24] D. Limebeer, G. Perantoni, and A. Rao, "Optimal control of formula one car energy recovery systems," *International Journal of Control*, vol. 87, no. 10, pp. 2065–2080, 2014. [Online]. Available: http://dx.doi.org/10.1080/00207179.2014.900705

[25] C. L. Darby, W. W. Hager, and A. V. Rao, "An hp-adaptive pseudospectral method for solving optimal control problems," *Optimal Control Applications and Methods*, vol. 32, no. 4, pp. 476–502, 2011.

[26] D. Garg, W. W. Hager, and A. V. Rao, "Pseudospectral methods for solving infinite-horizon optimal control problems," *Automatica*, vol. 47, no. 4, pp. 829 – 837, 2011. [Online]. Available: http://www.sciencedirect.com/science/article/pii/S0005109811001002

[27] G. L. Plett, "Extended kalman filtering for battery management systems of lipb-based {HEV} battery packs: Part 3. state and parameter estimation," *Journal of Power Sources*, vol. 134, no. 2, pp. 277 – 292, 2004. [Online]. Available: http://www.sciencedirect.com/science/article/pii/S0378775304003611

[28] I. S. Kim, "A technique for estimating the state of health of lithium batteries through a dual-sliding-mode observer," *IEEE Transactions on Power Electronics*, vol. 25, no. 4, pp. 1013–1022, April 2010.